

We are IntechOpen, the world's leading publisher of Open Access books Built by scientists, for scientists

6,900

Open access books available

186,000

International authors and editors

200M

Downloads

Our authors are among the

154

Countries delivered to

TOP 1%

most cited scientists

12.2%

Contributors from top 500 universities



WEB OF SCIENCE™

Selection of our books indexed in the Book Citation Index
in Web of Science™ Core Collection (BKCI)

Interested in publishing with us?
Contact book.department@intechopen.com

Numbers displayed above are based on latest data collected.
For more information visit www.intechopen.com



Basic Properties of Fine Particle (Dusty) Plasmas

Hiroo Totsuji

Abstract

Beginning with typical values of physical parameters, basic properties of the system of fine particles (dusts) in plasmas are summarized from the viewpoint of statistical physics. Mutual interactions and one-body *shadow* potential for fine particles are derived, and, by analytic treatments and numerical solutions of drift-diffusion equations, it is shown that one of their most important characteristics is the large enhancement of the charge neutrality in fine particle clouds. This observation leads to simple models for the structures of fine particle clouds under both microgravity and usual gravity. Due to large magnitudes of their charges and relatively low temperatures, fine particles are often in the state of strong coupling, and some interesting phenomena possibly expected in their system are discussed with concrete examples. Also reviewed is the shell model, a useful framework to obtain microscopic structures in strongly coupled Coulomb and Coulomb-like systems with specific geometry.

Keywords: interaction and one-body potential, drift-diffusion equations, charge neutrality enhancement, cloud models under microgravity/gravity, strong coupling, shell model

1. Introduction

Fine particle (dusty) plasmas are weakly ionized plasmas including fine particles (dusts) of micron sizes [1–5]. As the gas species, inert gases such as He, Ne, Ar, etc. are usually (but may be not exclusively) used: one of the reasons is that various phenomena can be analyzed without considering chemical reactions including neutral atoms or ions and values of physical parameters are mostly known or easily estimated. To generate plasmas, the rf or dc discharge is used, and fine particles are intentionally added by particle dispensers in most cases. In this chapter, fine particles will be referred to simply as “particles.”

As for experimental observations, particles of micron sizes scatter laser beams, and their orbits are easily followed, for example, by ccd cameras. In addition to the importance of (often not welcome) effects of the existence of particles in reacting plasmas applied in semiconductor processes, the relative easiness of observation might be one of the motives of investigation.

Particles immersed in plasmas obtain negative charges of large magnitudes: the thermal velocity of electrons is much larger than that of ions. Even though the interaction between particles are screened by surrounding plasma (composed of electrons and ions), particles are sometimes mutually strongly coupled, and many

phenomena in strongly coupled Coulomb or Coulomb-like systems are expected to be observed.

From the viewpoint of statistical physics, systems of particles resemble the Coulomb system with the charges of definite (negative) sign, the screening of charges by surrounding plasma being the most important difference from the pure Coulomb systems. The mutual interaction between particles is approximately given by the Yukawa or the screened Coulomb potential. The one-component plasma (OCP) is a typical model of Coulomb systems composed of charges of definite sign where the inert charges of opposite sign (the background charge) neutralize the particle charges. In fine particle plasmas, particle charges are screened and, at the same time, neutralized by the surrounding plasma.

Compared with electrons and ions, particles have macroscopic masses, and the gravity on the ground has significant influence on their behavior. In order to observe their generic properties, the experiments in the environment of microgravity have been and are performed on the International Space Station (ISS) as PK-3Plus and PK-4 Projects [6, 7].

The main topics in the statistical physics of fine particle plasmas may be the following:

- Charging of fine particles
- Interaction between particles and their microscopic structures
- Behavior of electrostatic potential under the existence of particles
- Effect of gravity
- Simple models of fine particle clouds under microgravity and usual gravity
- Effects of strong coupling

In what follows, we will discuss them as much as possible within a limited space.

2. Typical values of parameters

Here we show some typical values of important parameters related to fine particle plasmas discussed in this chapter. They are summarized in **Table 1**.

Since we have weakly ionized plasmas, the density of neutral atoms is much larger than that of electrons, ions, or particles. The neutral atom density n_n at the pressure p_n and the temperature T_n

$$n_n \sim 2.081 \cdot 10^{14} (p_n [\text{Pa}]) \left(\frac{0.03}{k_B T_n [\text{eV}]} \right) \text{ cm}^{-3} \quad (1)$$

is to be kept in mind in considering phenomena in fine particle plasmas. It is sometimes necessary to take the effects of collisions between neutral atoms and electrons and ions into account: the collision cross section σ gives the collision mean free path $\ell = 1/n_n \sigma$ and corresponding collision frequency. Typical values of cross sections and the mean free path in our range of energy are

$$\sigma_{\text{electron-neutral}} \sim 2 \cdot 10^{-16} \text{ cm}^2 \quad (\text{e} - \text{Ar}), \quad (2)$$

Quantities	Notation	Values
Electron density	n_e	$10^8 - 10^9 \text{ cm}^{-3}$
Ion density	n_i	$10^8 - 10^9 \text{ cm}^{-3}$
Electron temperature	T_e	$(1 - 5) \text{ eV}/k_B$
Ion temperature	T_i	300 K
Fine particle size	r_p	1 μm
Fine particle density	n_p	10^5 cm^{-3}
Fine particle temperature	T_p	300 K
Neutral gas pressure	p_n	$10 - 10^2 \text{ Pa}$
Neutral gas temperature	T_n	300 K

Table 1.
 Typical values of parameters of fine particle plasmas.

$$\sigma_{ion-neutral} \sim 1 \cdot 10^{-14} \text{ cm}^2 \quad (\text{Ar}^+ - \text{Ar}), \quad (3)$$

$$\ell \sim \frac{1}{(p_n[\text{Pa}])} \text{ cm} \quad (\text{Ar}^+ - \text{Ar}). \quad (4)$$

The neutral gas is considered to be at room temperature. The temperature of electrons T_e is often measured or reasonably extrapolated from the discharge conditions. As for the ion temperature T_i , on the other hand, we usually do not have measured values and implicitly assume it to be around room temperature. There exist experiments where the velocity of the ion motion suggests higher temperatures. Most of experimental results, however, seem to be compatible with the above assumption. It may be also justified by frequent collision with neutral atoms. The temperature of particles T_p can be measured by monitoring their motion, and the latter sometimes indicates rather high temperatures of even eVs. We here assume, however, that particles are also at room temperature, attributing apparent high temperatures to some instability.

As will be shown in Section 1.4, charges on particles are screened by the plasma of electrons and ions with characteristic screening or Debye lengths: the electron Debye lengths λ_e and ion Debye lengths λ_i are, respectively

$$\lambda_e \equiv \left(\frac{\epsilon_0 k_B T_e}{n_e e^2} \right)^{1/2} \sim 7.434 \cdot 10^{-2} (k_B T_e [\text{eV}])^{1/2} \left(\frac{10^8}{n_e [\text{cm}^{-3}]} \right)^{1/2} \text{ cm}, \quad (5)$$

$$\lambda_i \equiv \left(\frac{\epsilon_0 k_B T_i}{n_i e^2} \right)^{1/2} \sim 1.288 \cdot 10^{-2} \left(\frac{k_B T_i [\text{eV}]}{0.03} \right)^{1/2} \left(\frac{10^8}{n_i [\text{cm}^{-3}]} \right)^{1/2} \text{ cm}. \quad (6)$$

Since $T_e \gg T_i$, we have for the total screening length $\lambda = 1/k_D$ as

$$\lambda \equiv \left(\frac{1}{1/\lambda_e^2 + 1/\lambda_i^2} \right)^{1/2} \sim \lambda_i \sim 1.29 \cdot 10^2 \left(\frac{k_B T_i [\text{eV}]}{0.03} \right)^{1/2} \left(\frac{10^8}{n_i [\text{cm}^{-3}]} \right)^{1/2} \mu\text{m}. \quad (7)$$

The thermal velocity of electrons $v_{th,e}$ and that of ions $v_{th,i}$ for Ar^+ (Ar) are given, respectively, by

$$v_{th,e} \equiv \left(\frac{k_B T_e}{m_e} \right)^{1/2} \sim 4.194 \cdot 10^7 (k_B T_e [\text{eV}])^{1/2} \text{ cm/s}, \quad (8)$$

$$v_{th,i} \equiv \left(\frac{k_B T_i}{m_{Ar}} \right)^{1/2} \sim 2.692 \cdot 10^4 (k_B T_i [\text{eV}])^{1/2} \text{ cm/s}. \quad (9)$$

3. Charging of fine particles in plasmas

The charge on a particle $-Qe$ is one of the key parameters of our system. Since $v_{th,e} \gg v_{th,i}$, an object immersed in the plasma obtains negative charges. The resultant magnitude of the charge is determined so as to have balanced currents of electrons and ions onto the surface of particles. From the capacitance of a spherical capacitor of the radius r_p , $4\pi\epsilon_0 r_p$, and the potential difference $k_B T_e/e$, we have a rough estimate as $Qe \sim 4\pi\epsilon_0 r_p (k_B T_e/e)$. For micron-sized particles in the plasma with the electron temperature of the order of eV, the charge number Q easily has the magnitudes of $10^2 - 10^3$.

From the analysis of electron and ion currents, we have

$$Q = z \frac{k_B T_e}{e^2/4\pi\epsilon_0 r_p} = z \times 6.94 \cdot 10^2 (r_p [\mu\text{m}]) (k_B T_e [\text{eV}]), \quad (10)$$

where z is determined by

$$\exp(-z) = \frac{n_i}{n_e} \left(\frac{m_e}{m_{Ar}} \frac{T}{T_e} \right)^{1/2} \left[1 + \frac{T_e}{T_i} z + 0.1 \left(\frac{T_e}{T_i} \right)^2 z^2 \frac{\lambda}{\ell_i} \right]. \quad (11)$$

Here the first and second terms in [] on the right-hand side are given by the orbit-motion-limited (OML) theory [8, 9], and the third term is the effect of ion-neutral collisions, ℓ_i being the ion mean free path [10]. Typically this equation gives $z \sim 0.5$.

4. Mutual interaction and one-body potential in fine particle system

In the system composed of the electron-ion plasma and particles, we are mainly interested in the latter and take statistical average with respect to variables related to the former. Such a treatment of the uniform system was given previously [11, 12]. For systems of particles in plasmas considered here, however, the effects of nonuniformity are of essential importance. The corresponding inhomogeneous system has been analyzed, and mutual interactions and the one-body potential have been obtained [13]. In the process of statistical average, the importance of the charge neutrality of the whole system is pointed out. The main results are summarized below.

Since the thermal velocity of particles is much smaller than that of electrons or ions, we adopt the adiabatic approximation and regard configurations of particles as static. Under the conditions of fixed volume and fixed temperature, the work necessary to change the configuration of particles (the effective interaction) is given by the change in the Helmholtz free energy of the electron-ion system [14]. The effective interaction energy U_{ex} for particles is thus written as

$$U_{ex} = F_{id}^{(e)} + F_{id}^{(i)} + \left[\frac{1}{2} \int d\mathbf{r} \rho(\mathbf{r}) \Psi(\mathbf{r}) - U_s \right]. \quad (12)$$

Here, $F_{id}^{(e)} + F_{id}^{(i)}$ is the Helmholtz free energy of the electron-ion plasma

$$F_{id}^{(e,i)} = k_B T_{e,i} \int dr n_{e,i}(\mathbf{r}) (\ln [n_{e,i}(\mathbf{r}) \Lambda_{e,i}^3] - 1), \quad (13)$$

Λ_e and Λ_i being the thermal de Broglie lengths, $\rho(\mathbf{r})$ the charge density

$$\rho(\mathbf{r}) = \rho_p(\mathbf{r}) + \rho_{bg}(\mathbf{r}), \quad \rho_p(\mathbf{r}) = -Qe \sum_i \delta(\mathbf{r} - \mathbf{r}_i), \quad \rho_{bg}(\mathbf{r}) = en_i(\mathbf{r}) - en_e(\mathbf{r}), \quad (14)$$

and $\Psi(\mathbf{r})$ the electrostatic potential. (We subtract the self-energy $U_s = (1/2) \sum_{i=j}^N (-Qe)^2 / 4\pi\epsilon_0 r_{ij}$ formally included in the integral.) We apply the ideal gas value to $F_{id}^{(e)} + F_{id}^{(i)}$ assuming weakly coupled electron-ion plasma.

The (microscopic) particle charge density $\rho_p(\mathbf{r})$ fluctuates around the average $\overline{\rho_p(\mathbf{r})}$ as $\rho_p = \overline{\rho_p} + \delta\rho_p$ and induces the density fluctuations of electrons and ions. The potential also fluctuates as $\Psi = \overline{\Psi} + \delta\Psi$. We assume that electrons and ions respond to $\delta\Psi$ as (+ for e and $-$ for i)

$$\delta n_{e,i}(\mathbf{r}) \sim \overline{n_{e,i}(\mathbf{r})} \left[\exp\left(\pm \frac{e\delta\Psi(\mathbf{r})}{k_B T_{e,i}}\right) - 1 \right] \sim \pm \overline{n_{e,i}(\mathbf{r})} \frac{e\delta\Psi(\mathbf{r})}{k_B T_{e,i}} \quad (15)$$

and have

$$\delta\Psi(\mathbf{r}) \sim \int dr' u(\mathbf{r}, \mathbf{r}') \delta\rho_p(\mathbf{r}'), \quad (16)$$

where

$$u(\mathbf{r}, \mathbf{r}') = \frac{\exp(-k_D^+ |\mathbf{r} - \mathbf{r}'|)}{4\pi\epsilon_0 |\mathbf{r} - \mathbf{r}'|}, \quad k_D^+ = k_D [(\mathbf{r} + \mathbf{r}')/2], \quad (17)$$

with the screening parameter evaluated at the midpoint $(\mathbf{r} + \mathbf{r}')/2$ noting the position dependence of electron and ion densities.

We expand $F_{id}^{(e)} + F_{id}^{(i)}$ with respect to fluctuations to the second order as

$$\sim F_{id,0} + \frac{1}{2} \int dr \left[k_B T_e \frac{\delta n_e^2(\mathbf{r})}{\overline{n_e(\mathbf{r})}} + k_B T_i \frac{\delta n_i^2(\mathbf{r})}{\overline{n_i(\mathbf{r})}} \right] = F_{id,0} - \frac{1}{2} \int dr \delta\rho_{bg}(\mathbf{r}) \delta\Psi(\mathbf{r}), \quad (18)$$

where $\delta\rho_{bg}(\mathbf{r}) = e\delta n_i(\mathbf{r}) - e\delta n_e(\mathbf{r})$ and

$$F_{id,0} = k_B T_e \int dr \overline{n_e(\mathbf{r})} [\ln [\overline{n_e(\mathbf{r})} \Lambda_e^3] - 1] + k_B T_i \int dr \overline{n_i(\mathbf{r})} [\ln [\overline{n_i(\mathbf{r})} \Lambda_i^3] - 1]. \quad (19)$$

The electrostatic energy is written as

$$\frac{1}{2} \int dr \rho \Psi - U_s = \frac{1}{2} \int dr \left[\overline{\rho_p} + \overline{\rho_{bg}} + \rho_{ext} \right] \overline{\Psi} + \frac{1}{2} \int dr \left[\delta\rho_p + \delta\rho_{bg} \right] \delta\Psi - U_s. \quad (20)$$

From (18) and (20), we have finally

$$U_{ex} = F_{id,0} + \frac{1}{2} \int d\mathbf{r} \left[\overline{\rho_p}(\mathbf{r}) + \overline{\rho_{bg}}(\mathbf{r}) + \rho_{ext}(\mathbf{r}) \right] \overline{\Psi}(\mathbf{r}) + \left[\frac{1}{2} \int d\mathbf{r} \delta\rho_p(\mathbf{r}) \delta\Psi(\mathbf{r}) - U_s \right]. \quad (21)$$

The last term of (21) is rewritten as

$$\begin{aligned} \frac{1}{2} \iint d\mathbf{r} d\mathbf{r}' u(\mathbf{r}, \mathbf{r}') \left[\rho_p(\mathbf{r}) - \overline{\rho_p}(\mathbf{r}) \right] \left[\rho_p(\mathbf{r}') - \overline{\rho_p}(\mathbf{r}') \right] - U_s &= \frac{(Qe)^2}{2} \sum_{i,j=1}^N u(\mathbf{r}_i, \mathbf{r}_j) \\ -U_s - (-Qe) \sum_{i=1}^N \int d\mathbf{r}' u(\mathbf{r}_i, \mathbf{r}') \overline{\rho_p}(\mathbf{r}') + \frac{1}{2} \iint d\mathbf{r} d\mathbf{r}' u(\mathbf{r}, \mathbf{r}') \overline{\rho_p}(\mathbf{r}) \overline{\rho_p}(\mathbf{r}') &. \end{aligned} \quad (22)$$

The first two terms on the right-hand side of (22) reduce to the mutual Yukawa repulsion and the free energy stored in the sheath:

$$\frac{1}{2} \sum_{i,j=1}^N (Qe)^2 u(\mathbf{r}_i, \mathbf{r}_j) - U_s = \frac{(Qe)^2}{2} \sum_{i \neq j}^N u(\mathbf{r}_i, \mathbf{r}_j) - \frac{1}{2} \sum_{i=1}^N \frac{(Qe)^2 k_D(\mathbf{r}_i)}{4\pi\epsilon_0} \quad (23)$$

and the Helmholtz free energy is finally given by

$$\begin{aligned} U_{ex} = F_{id,0} + \frac{1}{2} \int d\mathbf{r} \left[\overline{\rho_p}(\mathbf{r}) + \overline{\rho_{bg}}(\mathbf{r}) + \rho_{ext}(\mathbf{r}) \right] \overline{\Psi}(\mathbf{r}) \\ + \left[\frac{1}{2} \sum_{i \neq j}^N (Qe)^2 u(\mathbf{r}_i, \mathbf{r}_j) + \sum_{i=1}^N (-Qe) \int d\mathbf{r}' u(\mathbf{r}_i, \mathbf{r}') \left[-\overline{\rho_p}(\mathbf{r}') \right] \right] \\ + \frac{1}{2} \iint d\mathbf{r} d\mathbf{r}' u(\mathbf{r}, \mathbf{r}') \overline{\rho_p}(\mathbf{r}) \overline{\rho_p}(\mathbf{r}') - \frac{1}{2} \sum_{i=1}^N \frac{(Qe)^2 k_D(\mathbf{r}_i)}{4\pi\epsilon_0}. \end{aligned} \quad (24)$$

The averages $\overline{\rho_p}(\mathbf{r})$, $\overline{\rho_{bg}}(\mathbf{r})$, and $\overline{\Psi}(\mathbf{r})$ are determined so as to be consistent with the plasma generation and loss and the ambipolar diffusion in the system (and also with the external potential, if any). Explicitly configuration-dependent terms in (24),

$$\frac{1}{2} \sum_{i \neq j}^N (Qe)^2 u(\mathbf{r}_i, \mathbf{r}_j) + \sum_{i=1}^N (-Qe) \int d\mathbf{r}' \left[-\overline{\rho_p}(\mathbf{r}') \right] u(\mathbf{r}_i, \mathbf{r}') - \frac{1}{2} \sum_{i=1}^N \frac{(Qe)^2 k_D(\mathbf{r}_i)}{4\pi\epsilon_0}, \quad (25)$$

describe the Helmholtz free energy for a given configuration of particles $\{\mathbf{r}_i\}_{i=1,\dots,N}$. The first term gives the mutual Yukawa repulsion between fine particles. The integral in the second term

$$\int d\mathbf{r}' \left[-\overline{\rho_p}(\mathbf{r}') \right] u(\mathbf{r}_i, \mathbf{r}') = \int d\mathbf{r}' \frac{\left[-\overline{\rho_p}(\mathbf{r}') \right]}{4\pi\epsilon_0 |\mathbf{r}_i - \mathbf{r}'|} \exp(-k_D^+ |\mathbf{r}_i - \mathbf{r}'|), \quad (26)$$

can be regarded as the Yukawa potential at \mathbf{r}_i due to $\left[-\overline{\rho_p}(\mathbf{r}') \right]$, the (imaginary) charge density, which exactly cancels the average particle charge density $\overline{\rho_p}(\mathbf{r}')$. We may call $\left[-\overline{\rho_p}(\mathbf{r}') \right]$ the *shadow* to $\left[\overline{\rho_p}(\mathbf{r}') \right]$. The charge density of the shadow has the sign opposite to that of particles, and the potential due to the shadow is attractive

for particles. Thus we may summarize the result as *particles are mutually interacting via the Yukawa repulsion and, at the same time, confined by the attractive potential due to the shadow charge density* $\left[-\overline{\rho_p}(\mathbf{r}')\right]$.

The last term in (24) and (25), the free energy stored in the sheath around each particle, works as a one-body potential for particles: this is called the polarization force [15].

5. Description by drift-diffusion equations

In Section 4, we have derived the effective interaction and the one-body *shadow* potential for particles. The behavior of average densities can be analyzed on the basis of the drift-diffusion equations [16, 17]. Here we derive average densities of electrons, ions, and particles and determine the one-body potential for particles [18–21] which enables microscopic simulations of fine particle distribution.

For densities $n_{e,i,p}$ and flux densities $\Gamma_{e,i,p}$, the equations of continuity are written in the form

$$\frac{\partial n_e}{\partial t} + \nabla \cdot \Gamma_e = \frac{\delta n_e}{\delta t}, \quad \frac{\partial n_i}{\partial t} + \nabla \cdot \Gamma_i = \frac{\delta n_i}{\delta t}, \quad \frac{\partial n_p}{\partial t} + \nabla \cdot \Gamma_p = 0, \quad (27)$$

where $\delta n_e/\delta t = \delta n_i/\delta t$ is the contribution of the plasma generation/loss. Flux densities are given by diffusion coefficients $D_{e,i,p}$ and mobilities $\mu_{e,i,p}$ as

$$\begin{aligned} \Gamma_e &= -D_e \nabla n_e - n_e \mu_e \begin{pmatrix} \mathbf{F}_e \\ -e \end{pmatrix}, & \Gamma_i &= -D_i \nabla n_i + n_i \mu_i \begin{pmatrix} \mathbf{F}_i \\ e \end{pmatrix}, \\ \Gamma_p &= -D_p \nabla n_p - n_p \mu_p \begin{pmatrix} \mathbf{F}_p \\ -Qe \end{pmatrix}. \end{aligned} \quad (28)$$

Here $\mathbf{F}_{e,i,p}$ are forces for an electron, an ion, and a particle, respectively. We assume Einstein relations between diffusion coefficients and mobilities

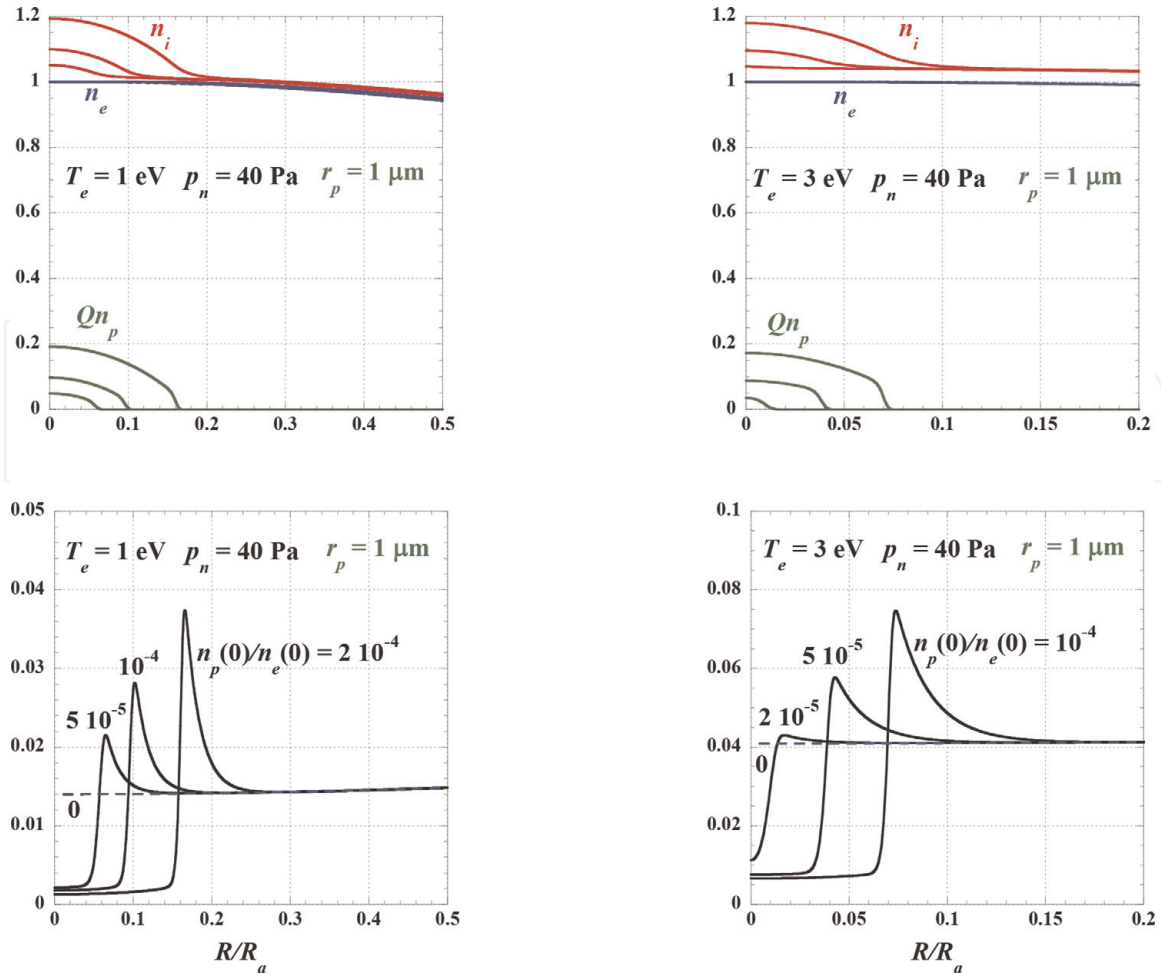
$$\frac{D_e}{\mu_e} = \frac{k_B T_e}{e}, \quad \frac{D_i}{\mu_i} = \frac{k_B T_i}{e}, \quad \frac{D_p}{\mu_p} = \frac{k_B T_p}{Qe} \quad (29)$$

with the temperature of each component, $T_{e,i,p}$. Solutions of (27) are characterized by the ambipolar diffusion length R_a . Forces $\mathbf{F}_{e,i,p}$ are due to the electric field, and, for \mathbf{F}_p , we also take the gravity $m_p \mathbf{g}$ and the ion drag force [22] into account: the reaction of the latter is to be included for ions but with small effect. We consider the stationary state.

5.1 Microgravity

We first neglect the gravity or consider the case under microgravity [18]. Examples of solutions of drift-diffusion equations are shown in **Figure 1** where we assume the cylindrical symmetry expecting applications to discharges in cylindrical tube. The main results are:

- a. The charge neutrality is largely enhanced in fine particle clouds.
- b. The ion distribution compensates the negative charge of particles.
- c. The electron distribution is not sensitive to the existence of particles.


Figure 1.

Examples of solutions of drift-diffusion equations under microgravity. On the left panel, from top, densities and the net charge density both normalized by $n_e(0)$ at $T_e = 1\text{eV}$. On the right panel, those at $T_e = 3\text{eV}$. Three cases are shown at each electron temperature [18].

The enhancement of the charge neutrality is shown also analytically [23]. We obtain the condition for the formation of voids around the center: voids are formed when the electron density is high and the neutral gas pressure is low and the radius of particles is large. The critical density is given approximately by [18]

$$n_e^{\text{critical}}(0) \sim 4 \times \frac{(p_n[\text{Pa}])^{1.56}}{(r_p[\mu\text{m}])^{0.42} (T_e[\text{eV}])^{0.24}} 10^6 \text{ [cm}^{-3}\text{]}. \quad (30)$$

5.2 Gravity

In the case under gravity, we have the same equations, but the effect of gravity is to be taken into account for the force on particles [20, 21]. The distributions do not have symmetries even in cylindrical discharges. Here we assume the one-dimensional structures: the assumption is applicable to the case under gravity at least at the central part of the distributions. Examples of solutions are shown in **Figure 2** [20, 21]. We also observe the large enhancement of the charge neutrality as in the case of microgravity. The enhancement is derived also analytically [24].

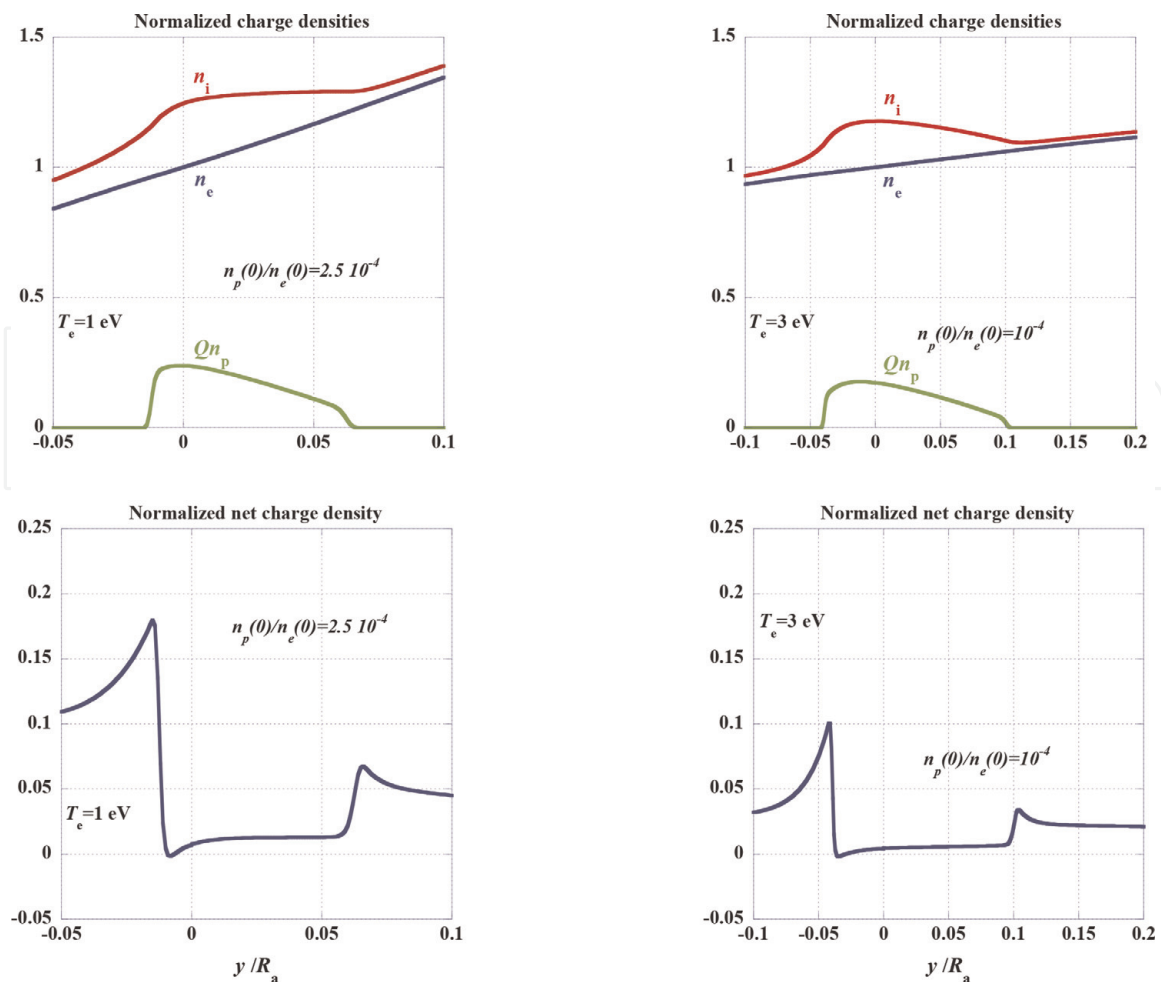


Figure 2.

Examples of solutions of drift-diffusion equations under gravity [21]. On the left panel, from top, densities and the net charge density both normalized by $n_e(0)$ at $T_e = 1$ eV. On the right panel, those at $T_e = 3$ eV. The origin $y = 0$ is (arbitrarily) taken in particle clouds. The slope of n_e and n_i outside of clouds corresponds to the electric field supporting particles against gravity.

6. Enhancement of charge neutrality in fine particle clouds: application to models

In clouds of particles, we have largely enhanced charge neutrality as in **Figures 1** and **2**, shown by numerical solutions of the drift-diffusion equations and analytically [18, 20, 21, 24]. This observation enables us to construct simple models of particle clouds in plasmas. The charge neutrality in the domain of fine particles' existence was noticed previously [25–27] but first established as one of the most important characteristics in particle clouds by our analyses.

6.1 Microgravity

In cylindrical fine particle plasmas under microgravity, particles gather around the center where the potential is maximum. Based on the enhanced charge neutrality in particle clouds, we are able to derive a relation between the radii of particle cloud and of the discharge tube from the boundary conditions of the potential. As shown in **Figure 3**, the cloud radius increases with the tube radius, and there exists a minimum of tube radius for the existence of the central cloud [23].

Cloud radius vs. plasma radius (cylindrical symmetry)

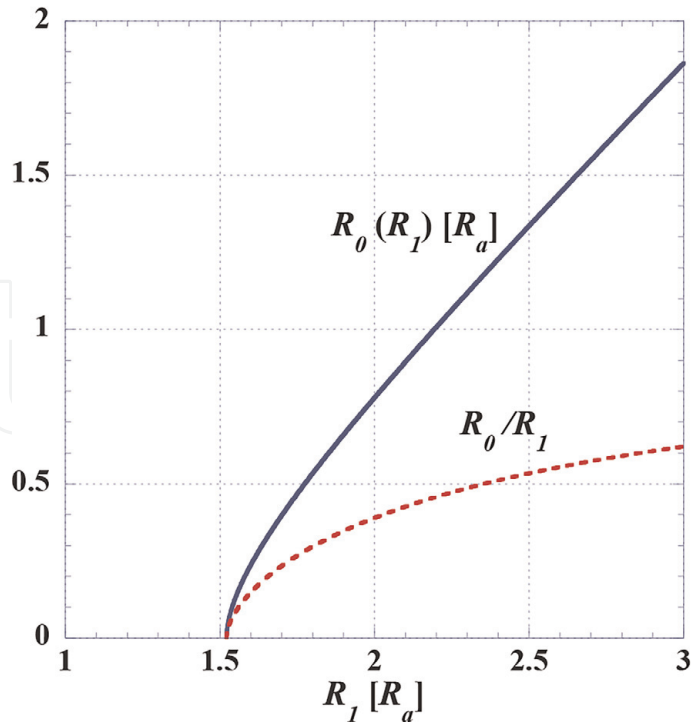


Figure 3. Cloud radius R_0 and ratio R_0/R_1 as functions of plasma radius R_1 , both radii in units of ambipolar diffusion length R_a [23].

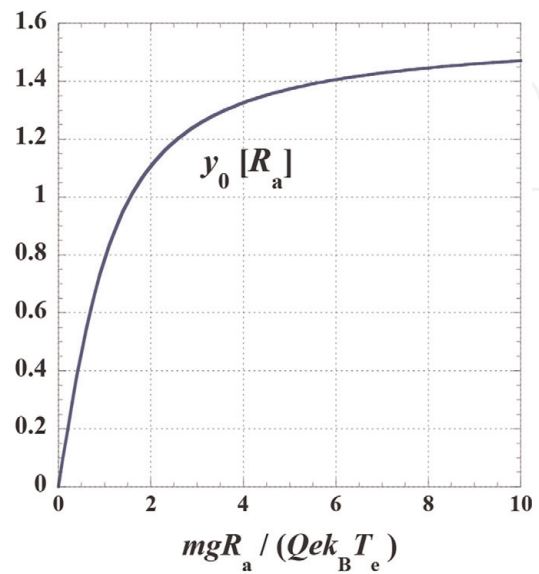
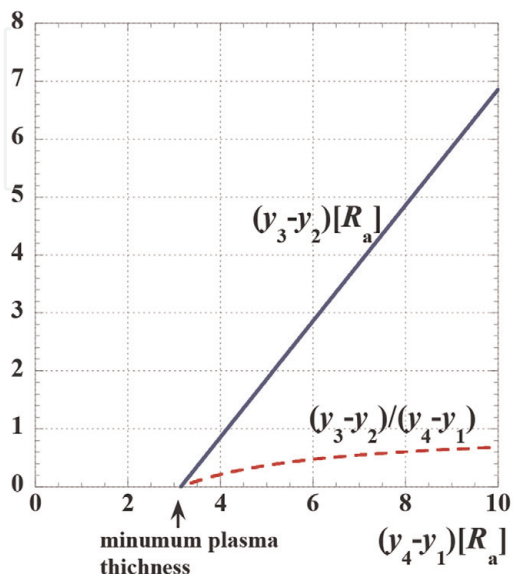
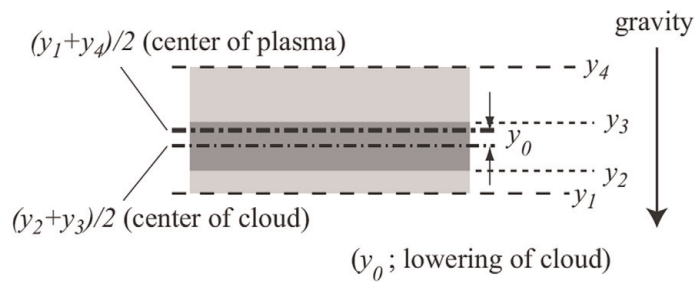


Figure 4. Particle cloud (dark gray) in plasma (light gray) under gravity (upper panel), cloud thickness (lower left), and lowering of cloud center (lower right) in units of R_a [24].

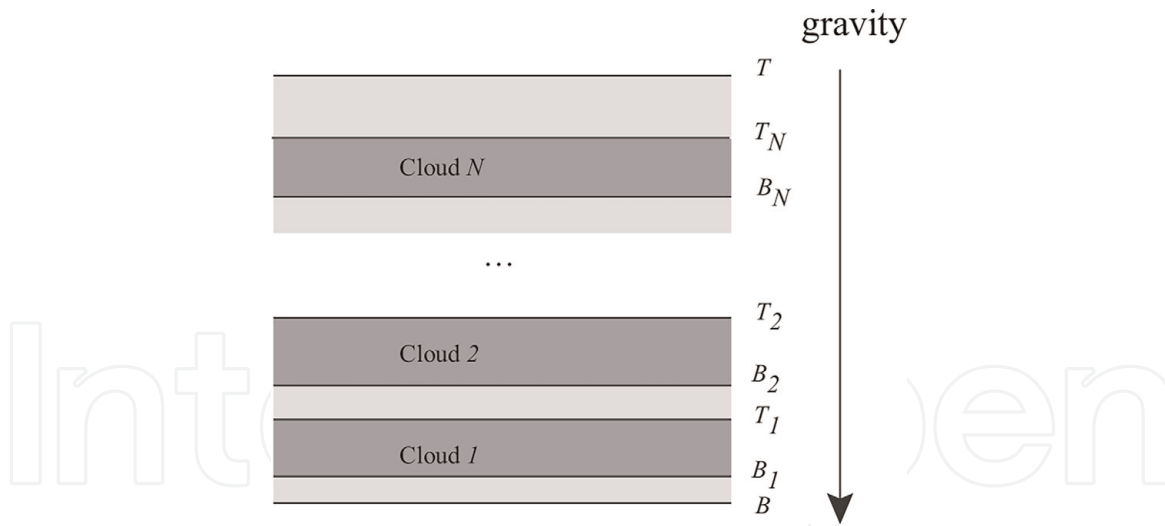


Figure 5. Stratified particle clouds under gravity. Clouds (between T_i and B_i) of different species are separated by the difference in $\tan^{-1}\left(\frac{m_i g R_p}{Q_i k_B T_e}\right)$ [28].

6.2 Gravity

In the case under gravity, we have a structure shown in the upper panel of **Figure 4**. In this case, the thickness of particle cloud is related to that of whole plasma as shown in the lower left panel, and the center of the cloud is located under the center of the whole plasma as in the lower right panel [24].

The result under gravity is extended to the case where we have multiple species of particles as shown in **Figure 5**. We have stratified clouds in the order of the charge/mass ratio, and the spacings are expressed by simple formulae [28].

7. Example of numerical simulations

For microscopic structures of Coulomb or Coulomb-like systems, there have been developed various theoretical methods including the ones applicable to inhomogeneous cases. Once the interaction and the one-body potentials for particles are established, however, numerical simulations of particle orbits may be the most useful. Their charges being screened by surrounding electron-ion plasma, particles mutually interact via the Yukawa repulsion. Since their charges are of the same (negative) sign, the system naturally tends to expand if we have no confinement.

In the case of infinite uniform system, one usually confines particles implicitly by imposing the periodic boundary conditions (with fixed volume). The number of particles being also fixed, we have effective background of smeared-out Yukawa particles with the opposite charge.

The necessity of confinement becomes clearer when one simulates finite and/or inhomogeneous systems. We here emphasize that, as shown in Section 4, particles are actually confined by the *shadow* potential corresponding to the average density of particles which, in principle, is to be determined self-consistently with the distribution of particles. It is also to be noted that, in addition to the *shadow* potential, there may exist additional external one-body potential, depending on experimental setups. In most cases, however, some kinds of parabolic confining potential or the

shadow potential for the expected average distribution have been assumed, and its self-consistency has not been rigorously achieved.

7.1 Microgravity

Under microgravity, we may assume simple symmetries of the system coming from the geometry of the apparatus. The cylindrical symmetry is one such common example.

From the result of the drift-diffusion analyses, we expect the formation of clouds of fine particles around the symmetry axis. In the cloud, we have almost flat electrostatic potential due to enhanced charge neutrality in clouds. Microscopic structure of particles in the cloud can be obtained by numerical simulations.

Before drift-diffusion analyses, microscopic structures have been analyzed by assuming the *shadow* potential corresponding to the uniform distribution of particles [29]. This shadow potential is not exact but almost identical to the real one. The assumed uniform average distribution and the shadow potential are shown in **Figure 6**.

At low temperatures, particles take shell structures as shown in **Figure 7**, and these structures are expressed by simple interpolation formulae [29]. One may almost justify *a posteriori* the *shadow* potential corresponding to flat average distribution which was assumed in advance of the analysis given in Section 4.

7.2 Gravity

Examples of the potential under gravity are given by drift-diffusion analyses shown in **Figure 2** [20, 21]: potentials (not shown in figures) correspond to the almost charge-neutral density distribution in particle clouds. Microscopic distribution of particles has been simulated by assuming the *shadow* potential given by the drift-diffusion analysis as shown in **Figure 8** [20]. In this case, parameters approximately correspond to the case shown in the left part of **Figure 2**, and particles are organized into two horizontal layers.

Though the *shadow* potential has to be determined self-consistently, there may be the case where particles are vertically confined by a given potential: with the

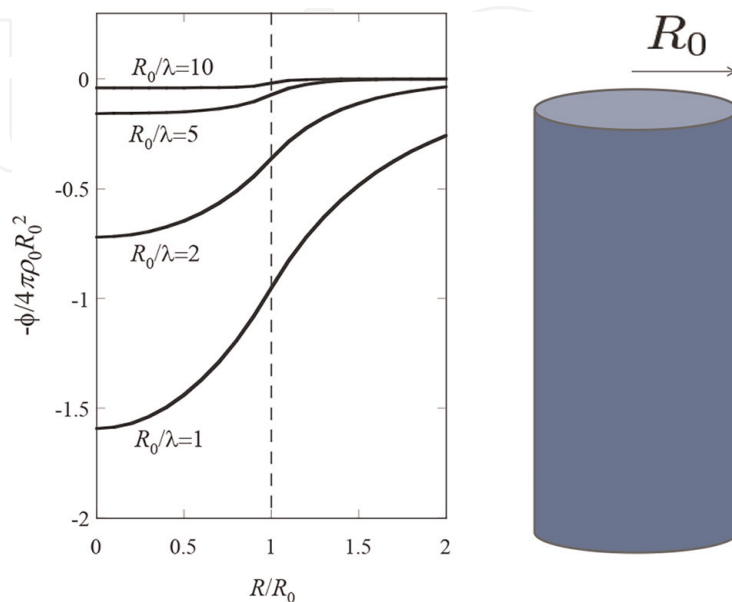
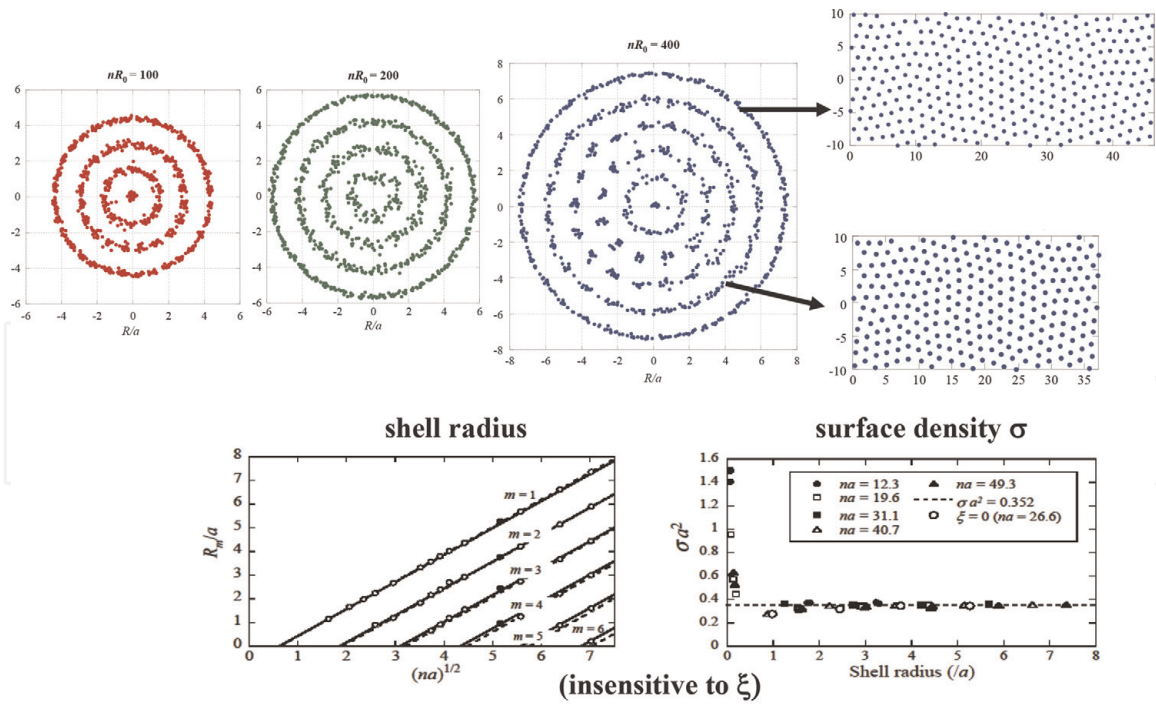


Figure 6. Assumed shadow potential for simulations (left) and corresponding to uniform cylindrical distribution (right) [29].



interpolation formulas for structures

$$R_m/a = 1.138 (na)^{1/2} - 1.411 (m - 0.501) \quad d/a = 1.411 \quad \sigma a^2 \sim 0.352$$

Figure 7.

Shell structures under microgravity in the shadow potential of **Figure 6**. Particles are ordered into triangular lattice with defects of almost equal density in each shell, and shell radius is expressed by simple interpolation formula [29].

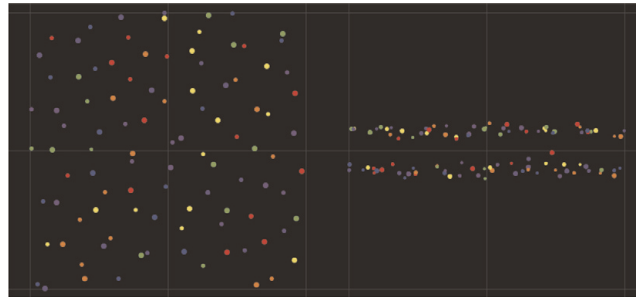


Figure 8.

Horizontal (left) and vertical (right) distributions of particles in a cloud under downward gravity (with colors for identification) [20]. Parameters correspond to the left panel of **Figure 2** [20, 21].

effect of the gravity, we may assume a one-dimensional parabolic confining potential. In this case, the structure of particle cloud at low temperatures is determined by the relative strength of the confinement and the mutual repulsion:

$$v(z) = \frac{1}{2}kz^2 \quad \text{vs.} \quad \frac{(Qe)^2}{4\pi\epsilon_0 r} \exp(-r/\lambda) \quad (31)$$

At low temperatures, particles form horizontal layers, and the number of layers is shown in a phase diagram in **Figure 9** [30]. Parameters characterizing strengths of confinement η and screening ξ are defined, respectively, by

$$\eta = \frac{k}{[(Qe)^2/\epsilon_0] N_S^{3/2}} = \frac{kN_S^{-1}}{(Qe)^2/\epsilon_0 N_S^{-1/2}} = \frac{\text{confinement}}{\text{repulsion}}, \quad (32)$$

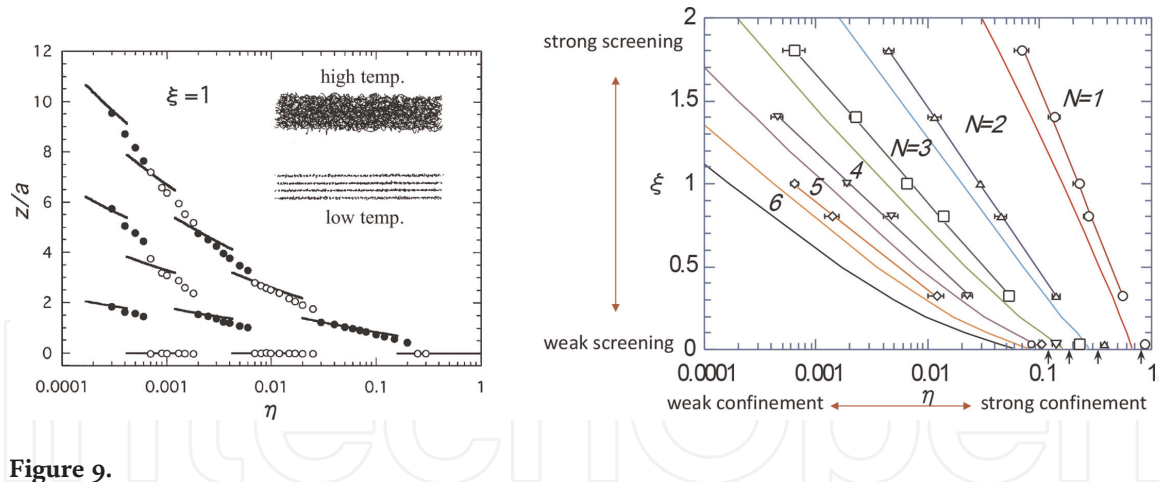


Figure 9. Yukawa system confined by a parabolic potential. Layered structure (left) and phase diagram for number of layers (right). Dots are numerical simulation and lines are results of shell model [30].

$$\xi = \frac{1}{(\pi N_S)^{1/2} \lambda} = \frac{(\pi N_S)^{-1/2}}{\lambda} = \frac{\text{mean distance}}{\text{screening length}}. \quad (33)$$

Note that the mean distance $a = (\pi N_S)^{-1/2}$ defined by the total areal density N_S is used for characterization.

Results of simulations are reproduced by the shell model to a good accuracy (see Appendix).

8. Aspects as strongly coupled system

The system of particles with the Yukawa mutual interaction

$$\frac{(Qe)^2}{4\pi\epsilon_0 r} \exp(-r/\lambda) \quad (34)$$

has long been explored as a model which interpolates systems with the short-ranged and long-ranged interactions [31]. Since particles of the same charge repel each other, the existence of the uniform *shadow* potential is (often implicitly) assumed. There are three phases at thermal equilibrium: fluid, bcc lattice, and fcc lattice. The parameters Γ and ξ defined, respectively, by

$$\Gamma = \frac{1}{k_B T} \frac{(Qe)^2}{4\pi\epsilon_0 a}, \quad \xi = \frac{a}{\lambda}, \quad (35)$$

a being the mean distance defined by the particle density $(4\pi a^3/3)n_p = 1$, characterize the system, and the phase diagram takes the form shown in **Figure 10** (ξ differs from the one defined by (33)). In computer simulations with a fixed number of particles and periodic boundary conditions with fixed shape or the volume of the fundamental cell, the existence of the *shadow* potential coming from the uniform average particle density is automatically built in.

When the coupling parameter Γ is sufficiently large and the screening is not so strong, the pressure obtained by these analyses of the Yukawa system takes on negative values, and the isothermal compressibility even diverges. Negative pressures may sound somewhat strange for this system with repulsion, but it is to be noted that the pressure obtained by these analyses of the Yukawa system is

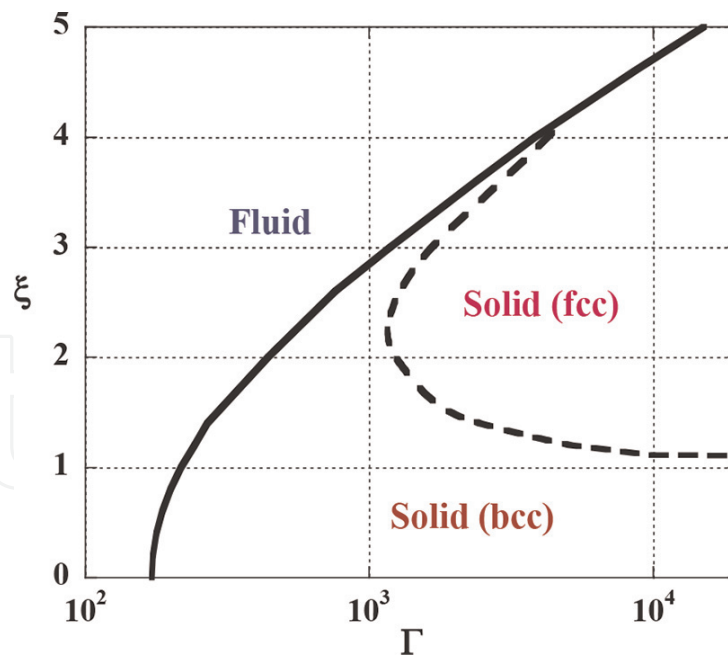


Figure 10.
 Phase diagram of Yukawa system.

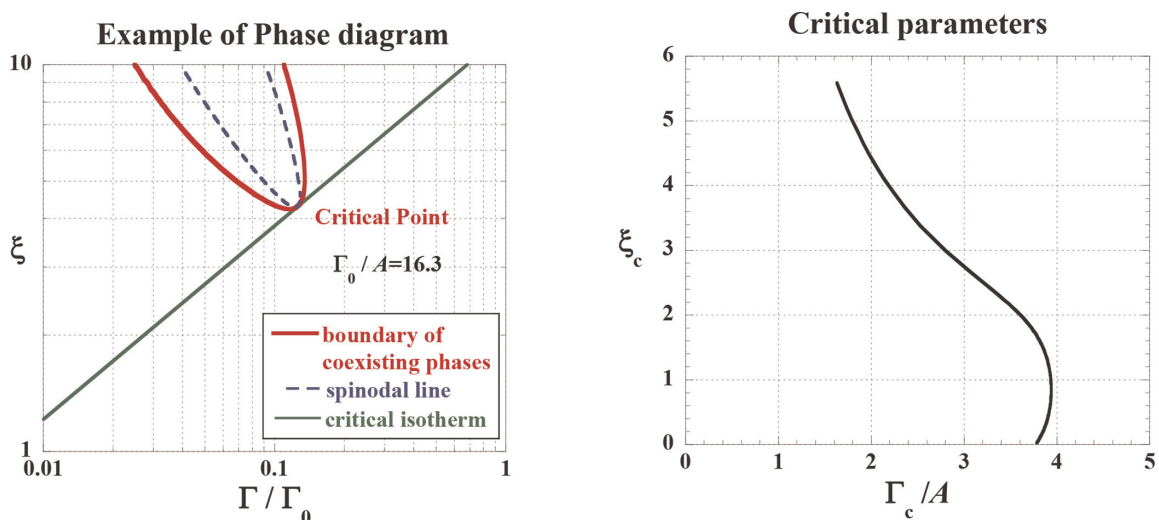


Figure 11.
 Example of phase diagram of fine particle plasma [33].

assuming the deformation of the *shadow* potential without any cost of energy. In reality, we have the surrounding plasma which has positive pressure of sufficient magnitude, and these negative pressures usually cannot be observed.

In fine particle plasmas, the magnitude of particle charge can become very large, and we have a possibility of negative pressures and divergent isothermal compressibility of the whole system including the surrounding plasma [32]. As physical phenomena, the latter is very interesting, and the corresponding conditions have been predicted [33]. An example of the phase diagram is shown in the left panel of **Figure 11**. Here A is the ratio of the ideal gas pressure of the surrounding plasma (electrons and ions) to the ideal gas pressure of particles and is usually much larger than unity, and Γ_0 is defined similarly to Γ with a replaced by the radius of particle. The locus of the critical point in (Γ, ξ) -plane is shown in the right panel of **Figure 11**.

Along these considerations, the enhancement of long wavelength fluctuations of density has been expected in the PK-3Plus experiments on ISS, but, since the nonuniformity of the system (particle cloud) gives similar behavior of the fluctuation spectrum, the results have not been conclusive.

9. Conclusions

In this chapter, we have discussed important aspects of fine particle systems immersed in fine particle (dusty) plasmas from the viewpoint of basic physics. We have introduced them as an example of many body system, which allows direct observations of orbits of constituent particles. Mutual interactions and one-body potential for particles are derived on the basis of statistical mechanics, and the enhancement of charge neutrality in fine particle clouds is emphasized as a basis for constructing models of structures. Due to large magnitudes of fine particle charges, these systems have a possibility to manifest some interesting but not yet observed phenomena related to the strongly coupled Coulomb or Coulomb-like systems. They are also discussed with concrete examples.

Fine particles show various interesting dynamic behaviors which are not included in this chapter of limited space. From a theoretical point of view, we would like to stress the importance of understanding the structure of the electrostatic potential and distributions of electrons and ions which are usually not directly observable but are playing a fundamental role to determine the visible behavior of particles.

Acknowledgements

The author would like to thank organizers/participants of series of Workshop on Fine Particle Plasmas supported by the National Institute for Fusion Science (NIFS), Japan, for useful information exchange. For discussions, he is also indebted to Dr. K. Takahashi, Dr. S. Adachi, and the members of the previous ISAS/JAXA Working Group of dusty plasma microgravity experiments (supported by Japan Aerospace Exploration Agency). In relation to the PK-3Plus project, thanks are due to members of the Max Planck Institute for Extraterrestrial Physics (MPE) and Joint Institute for High Temperatures (JIHT, RAS), especially to Professor G. Morfill, Dr. H. Thomas, and Professor V. E. Fortov, including the late Dr. Vladimir Molotkov.

Appendix: Shell model for Coulomb and Coulomb-like systems

When the temperature is sufficiently low, particles are organized into some kind of lattice structures. In the case of uniform system, it is not difficult to determine the structure with the lowest energy. When the symmetry of the system is restricted by the geometry of boundary conditions, however, it is not so easy to determine the lowest energy state theoretically. For Coulomb or Coulomb-like systems, the shell model which has been first proposed for the structure analysis of ions in traps [34] is known to reproduce low-temperature structures to a good accuracy [35].

This model consists of three steps:

1. Assume that particles are organized into a collection of two-dimensional systems (generally not-planar sheets) which are in accordance with the symmetry of the system.
2. Calculate the energy taking the cohesive energy in sheets into account.
3. Minimize the energy of the system with respect to all parameters, the number of sheets, number densities in the sheets, and positions of sheets.

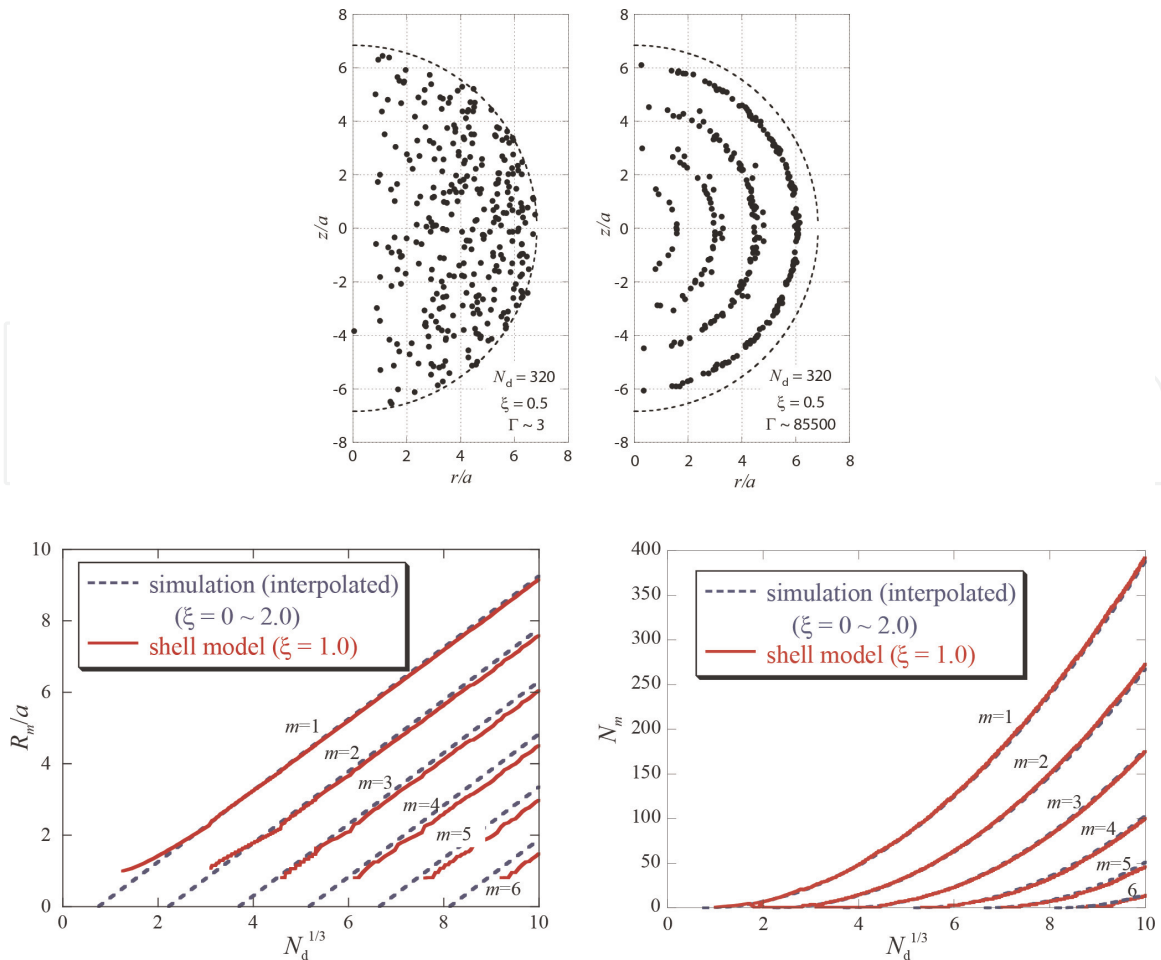


Figure 12. Example of shell formation (upper panel), radii of shells (lower left), and number of particles on each shell (lower right). In lower panel, simulation results are expressed by interpolated expression [37].

In the above steps, the consideration of the two-dimensional cohesive energy is essential: without its contribution (which have a negative contribution of magnitudes increasing with the density in sheets), we have infinite number of sheets with infinitely low density at the ground state. We can reproduce numerical simulation or real experiments in the cases of Coulomb system in a cylindrically symmetric confining potential [34], Yukawa system in a one-dimensional confining potential, [30] and Yukawa system in a spherically symmetric confinement (Coulomb ball) [36–38].

An example of three-dimensional confinement by the *shadow* potential corresponding to uniform average distribution is shown in **Figure 12** [36, 37]. The case of four shells is in agreement with the experiment [38], and simulation results are reproduced by the shell model to a good accuracy [37].

IntechOpen

IntechOpen

Author details

Hiroo Totsuji^{1,2}

1 Okayama University (Professor Emeritus), Okayama, Japan

2 Saginomiya, Nakanoku, Tokyo, Japan

*Address all correspondence to: totsuji-09@t.okadai.jp

IntechOpen

© 2020 The Author(s). Licensee IntechOpen. This chapter is distributed under the terms of the Creative Commons Attribution License (<http://creativecommons.org/licenses/by/3.0>), which permits unrestricted use, distribution, and reproduction in any medium, provided the original work is properly cited. 

References

- [1] Shukla PK, Mamun AA. Introduction to Dusty Plasma Physics. London: Institute of Physics Publishing; 2002
- [2] Fortov VE, Ivlev AV, Khrapak SA, Khrapak AG, Morfill GE. Complex (dusty) plasmas: Current status, open issues, perspectives. *Physics Reports*. 2005;**421**:1
- [3] Tsytovich VN, Morfill GE, Vladimirov SV, Thomas H. Elementary Physics of Complex Plasmas. Berlin, Heidelberg: Springer; 2008
- [4] Morfill GE, Ivlev AV. Complex plasmas: An interdisciplinary research field. *Reviews of Modern Physics*. 2009; **81**:1353
- [5] Fortov VE, Morfill GE, editors. Complex and Dusty Plasmas-From Laboratory to Space. Boca Raton, London, New York: CRC Press/Taylor and Francis Group; 2010
- [6] Fortov V, Morfill G, Petrov O, Thoma M, Usachev A, Höfner H, et al. The project 'Plasmakristall-4' (PK-4)—a new stage in investigations of dusty plasmas under microgravity conditions: first results and future plans. *Plasma Physics and Controlled Fusion*. 2005;**47**: B537
- [7] Thomas HM, Morfill GE, Fortov VE, Ivlev AV, Molotkov VI, Lipaev AM, et al. Complex plasma laboratory PK-3 plus on the international space station. *New Journal of Physics*. 2008;**10**:033036
- [8] Allen JE. Probe theory - the orbital motion approach. *Physica Scripta*. 1992; **45**:497
- [9] Goree J. Charging of particles in a plasma. *Plasma Sources Science and Technology*. 1994;**3**:400
- [10] Khrapak SA, Ratynskaia SV, Zobnin AV, Usachev AD, Yaroshenko VV, Thoma MH, et al. Particle charge in the bulk of gas discharges. *Physical Review E*. 2005;**72**: 016406
- [11] Hamaguchi S, Farouki RT. Thermodynamics of strongly-coupled Yukawa systems near the one-component-plasma limit. I. Derivation of the excess energy. *The Journal of Chemical Physics*. 1994;**101**:9876
- [12] Rosenfeld Y. Adiabatic pair potential for charged particulates in plasmas and electrolytes. *Physical Review E*. 1994;**49**:4425
- [13] Totsuji H. Modeling fine-particle (dusty) plasmas and charge-stabilized colloidal suspensions as inhomogeneous yukawa systems. *Journal of the Physical Society of Japan*. 2015;**84**:064501
- [14] Landau LD, Lifshitz EM. *Statistical Physics, Part 1*. 3rd ed. Oxford: Pergamon Press; 1980. Sect. 20
- [15] Hamaguchi S, Farouki RT. Polarization force on a charged particulate in a nonuniform plasma. *Physical Review E*. 1994;**49**:4430
- [16] Land V, Goedheer WJ. Effect of large-angle scattering, ion flow speed and ion-neutral collisions on dust transport under microgravity conditions. *New Journal of Physics*. 2006;**8**(8)
- [17] Goedheer WJ, Land V. Simulation of dust voids in complex plasmas. *Plasma Phys. Control. Fusion*. 2008;**50**:124022
- [18] Totsuji H. Distribution of electrons, ions, and fine (dust) particles in cylindrical fine particle (dusty) plasmas: drift-diffusion analysis. *Plasma Physics and Controlled Fusion*. 2016;**58**:045010
- [19] A part of preliminary result has been given in Totsuji H. Behavior of dust

particles in cylindrical discharges: Structure formation, mixture and void, effect of gravity. *Journal of Plasma Physics*. 2014;**80**(part 6):843

[20] Totsuji H. Strongly coupled fine particle clouds in fine particle (dusty) plasmas. *Contributions to Plasma Physics*. 2017;**57**:463

[21] Totsuji H. Static behavior of fine particle clouds in fine particle (dusty) plasmas under gravity. *Journal of Physics Communications*. 2018;**2**:025023

[22] Khrapak SA, Ivlev AV, Morfill GE, Thomas HM. Ion drag force in complex plasmas. *Physical Review E*. 2002;**66**:046414

[23] Totsuji H. Simple model for fine particle (dust) clouds in plasmas. *Physics Letters A*. 2016;**380**:1442

[24] Totsuji H. Charge neutrality of fine particle (dusty) plasmas and fine particle cloud under gravity. *Physics Letters A*. 2017;**381**:903

[25] Polyakov DN, Shumova VV, Vasilyak LM, Fortov VE. Influence of dust particles on glow discharge. *Physica Scripta*. 2010;**82**:055501

[26] Polyakov DN, Shumova VV, Vasilyak LM, Fortov VE. Study of glow discharge positive column with cloud of disperse particles. *Physics Letters A*. 2011;**375**:3300

[27] Sukhinin GI, Fedoseev AV, Antipov SN, Petrov OF, Fortov VE. Dust particle radial confinement in a dc glow discharge. *Physical Review E*. 2013;**87**:013101

[28] Totsuji H. One-dimensional structure of multi-component fine particle (dust) clouds under gravity. *Physics Letters A*. 2019;**383**:2065

[29] Totsuji H, Totsuji C. Structures of yukawa and coulomb particles in cylinders: Simulations for fine particle

plasmas and colloidal suspensions. *Physical Review E*. 2011;**84**:015401

[30] Totsuji H, Kishimoto T, Totsuji C, Tsuruta K. Structure of confined yukawa system (dusty plasma). *Physical Review Letters*. 1997;**78**:3113

[31] For example, Robbins MO, Kremer K, Grest GS. Phase diagram and dynamics of Yukawa systems. *Journal of Chemical Physics*. 1988;**88**:3286 and references therein

[32] Totsuji H. Thermodynamic instability and critical fluctuations in dusty plasmas modelled as yukawa OCP. *Journal of Physics A: Mathematical and General*. 2006;**39**:4565

[33] Totsuji H. Thermodynamics of strongly coupled repulsive yukawa particles in ambient neutralizing plasma: Thermodynamic instability and the possibility of observation in fine particle plasmas. *Physics of Plasmas*. 2008;**15**:072111

[34] Totsuji H, Barrat J-L. Structure of a nonneutral classical plasma in a magnetic field. *Physical Review Letters*. 1988;**60**:2484

[35] Dubin DHE, O'Neil TM. Trapped nonneutral plasmas, liquids, and crystals (the thermal equilibrium states). *Reviews of Modern Physics*. 1999;**71**:87

[36] Totsuji H, Totsuji C, Ogawa T, Tsuruta K. Ordering of dust particles in dusty plasmas under microgravity. *Physical Review E*. 2005;**71**:045401(R)

[37] Totsuji H, Ogawa T, Totsuji C, Tsuruta K. Structure of spherical yukawa clusters: A model for dust particles in dusty plasmas in an isotropic environment. *Physical Review E*. 2005;**72**:036406

[38] Arp O, Block D, Piel A, Melzer A. Dust coulomb balls: Three-dimensional plasma crystals. *Physical Review Letters*. 2004;**93**:165004